Accurate and emergent applications for high precision light small aerial remote sensing system

LIU Pei ,[1] **LI Yingcheng** [1,2] **, XUE Yanli** [1,2] **, HU Qingwu** [3] **, SUN Xiaofeng**[1]

[1] China TopRS Technology Co.,Ltd, Beijing, China.

[2] Chinese Academy of Surveying and Mapping, Beijing, China.

[3] Wuhan University, Wuhan, China.

E-mail: liupei@casm.ac.cn

Abstract. In this paper, we focus on the successful applications of accurate and emergent surveying and mapping for high precision light small aerial remote sensing system. First, the remote sensing system structure and three integrated operation modes will be introduced. It can be combined to three operation modes depending on the application requirements. Second, we describe the preliminary results of a precision validation method for POS direct orientation in 1:500 mapping. Third, it presents two fast response mapping products- regional continuous three-dimensional model and digital surface model, taking the efficiency and accuracy evaluation of the two products as an important point. The precision of both products meets the 1:2 000 topographic map accuracy specifications in Pingdingshan area. In the end, conclusions and future work are summarized.

1. Introduction

High resolution, good precision, flexible response and low cost always have been the goals of photogrammetry and remote sensing system development. In this paper, a new kind of system, called high precision light small aerial remote sensing system, will be introduced with advantage of low-altitude, high-precision survey and rapid response. The system plays an irreplaceable role in earth observation, compared with satellite remote sensing and conventional aerial photogrammetry.

There exist challenges of data processing for the new aerial remote sensing system. How to verify the stability, accuracy, quality and practical ability of the system in data processing stages will be the focal topic in this paper. It describes the successful applications in 1:500 mapping and fast response mapping for the system which includes a variety of new domestic advanced sensors.

2. High precision light small aerial remote sensing system

This remote sensing system consists of several domestic advanced sensors, such as two kinds of digital aerial photographic cameras, small-sized airborne Light Detection And Ranging (LiDAR), two kinds of IMU/GNSS systems and two types of stable platforms (also known as mounts). The remote sensing system can be combined to three operation modes (shown in Figure 1) depending on the application requirements.

Figure 1. The three operation modes of the high precision light small aerial remote sensing system
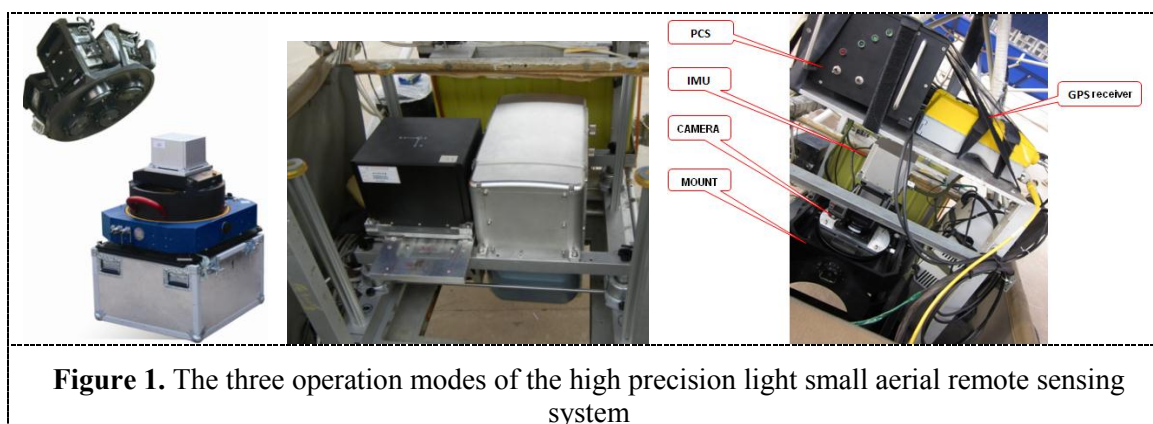
The first mode of the remote sensing system consists of wide-angle digital aerial photographic camera, high precision IMU/GNSS system and high precision large-load stable platform, which mainly applies to large-scale mapping, 3D modelling and precise measurement for geographic products of vector data, digital elevation models (DEM) , digital orthophoto maps (DOM) and others. For accurate terrain and other precise elevation applications, the second mode will hold superiority, which consists of LiDAR, high precision IMU/GNSS system and single-lens camera. In the field of emergency and disaster detection, the third mode including single-lens camera, miniaturized IMU/GNSS system and fast response stable platform, conforms to fast and low precision processing needs of DEM and DOM.

This system successfully realized unmanned aerial work with the help of flight management system，mission planning system and aerial quality inspection system. The remote sensing data can be processed in the same day of data obtaining.

3. A precision validation method for POS direct orientation in 1:500 mapping

Stereo mapping with image exterior orientation elements derived from POS observed values is a normal method of precision validation for POS direct orientation. However, the exterior orientation elements have already been integrated with multi-sensor system calibration errors. Point selecting and pricking errors exist as well. Only mapping with image exterior orientation elements can not evaluate POS direct orientation objectively and comprehensively. This paper presents a multi-level accuracy verification method in different data processing stages. 1:500 surveying and mapping experiment in Pingdingshan area for the remote sensing system was finished by considering the comparison based on position observations and aerial triangulation exterior orientation elements (level 1), POS direct orientation exterior orientation elements and aerial triangulation exterior orientation elements (level 2), multi-chip space intersection results and control points values (level 3), and stereo mapping results and control points values (level 4). The experimental data were obtained by high precision light small aerial remote sensing system with operation mode 1 in Pingdingshan, Henan Province, with the image resolution of 0.1m, flight height of 580m.

In level 1, there is a strong correlation between position observations exported from IMU/GNSS system and aerial triangulation exterior orientation elements which can be calculated from a few control points. For the reason that sensors in the aerial system are closely connected, the deviation between the two kinds of data should be a type of systematic errors. The stability of the deviation can characterize the accuracy and reliability of the IMU/GNSS system. Differences statistics between position observations and aerial triangulation exterior orientation elements are shown in Table 1.

Table 1. Differences statistics between position observations and aerial triangulation exterior orientation elements.

	Mean	Standard deviation
Δ φ（°）	-0.017	0.081
Δ ω（°）	-0.023	0.082
Δ κ（°）	-90.886	0.010
Δ X（m）	-0.042	0.044
Δ Y（m）	-0.006	0.020
Δ Z（m）	-0.487	0.037

In level 2, after system calibration with position and angle placement calculation for POS, camera and other sensors in the aerial remote sensing system, POS observations can be converted into camera position exterior orientation elements. The diversity between POS direct orientation exterior orientation elements and aerial triangulation exterior orientation elements can reflect the accuracy of the entire system (shown in table 2). The comparison between the two levels' results demonstrate that after calibration the angle elements' accuracy of the camera orientation exterior elements has improved to some extent.

Table 2. Differences statistics between POS direct orientation exterior orientation elements and aerial triangulation exterior orientation elements

	Mean	Standard deviation
△φ（°）	0.003	0.0038
△ω（°）	0.0017	0.0022
△κ（°）	-0.0004	0.0020
△X（m）	-0.037	0.044
△Y（m）	-0.007	0.020
△Z（m）	-0.005	0.037

In this paper, we make use of stereo image pairs with high-precision POS direct orientation information to carry out a multi-chip space intersection experiment with control points based on collinear equation shown in equation 1. Differences statistics between multi-chip space intersection results and control points values are shown in Table 3.

$$(x - x_0) = -f \frac{a_1(X - Xs) + b_1(Y - Ys) + c_1(Z - Zs)}{a_3(X - Xs) + b_3(Y - Ys) + c_3(Z - Zs)}$$
$$(y - y_0) = -f \frac{a_2(X - Xs) + b_2(Y - Ys) + c_2(Z - Zs)}{a_3(X - Xs) + b_3(Y - Ys) + c_3(Z - Zs)}$$

(1)

Table 3. Control point coordinates differences.

	△X	△Y	△Z
Max(m)	0.037	0.044	0.110
Mean(m)	-0.008	0.007	-0.031
Standard Deviation (m)	0.018	0.019	0.031

In level 4, with the exterior orientation elements derived from POS direct orientation, 1:500 scale topographic maps would be made by stereoscopic observation for detail point coordinates after the steps of relative orientation and absolute orientation. Further validation of POS direct orientation accuracy for large scale mapping will be evaluated by comparing coordinates of detail points and GPS points as true values. In the multi-level experiments all above, the control points are used only for accuracy validation instead of participation in POS direct orientation, relative orientation, absolute orientation and mapping stages. The experiment shows that, without control points, the topographic maps with horizontal accuracy of 11 centimetres and vertical accuracy of 7 centimetres can meet 1:500 accuracy requirements.

Table 4. Control point coordinates differences.

	△X	△Y	△Z
Max(m)	0.273	0.299	0.249
Mean(m)	-0.008	0.000	-0.052
Standard Deviation (m)	0.071	0.083	0.07

4. Regional continuous three-dimensional model and digital surface model

With the demand of fast response, this paper presents two fast response mapping products- regional continuous three-dimensional model and digital surface model, taking the efficiency and accuracy evaluation of the two products as an important point. Both products can express terrain and topography information vividly and rapidly, which can offer help of spatial representation, analysis and emergency decision.

Regional continuous three-dimensional model is a kind of model which allows the regional aerial image data sets in a certain area rather than one image pair to be automatically converted to three-dimensional model in real time, with visual impacts and analysis functions. The experimental data were obtained by high precision light small aerial remote sensing system in Pingdingshan. In order to verify the accuracy of regional continuous three-dimensional model, a number of points would be selected in experimental areas to complete accuracy verification tests(shown in table 5). With aerial digital image resolution of 10 cm, the processing speed of the regional continuous three-dimensional model can be $0.25h/km^2$, and the precision can meet 1:2000 topographic map accuracy specifications.
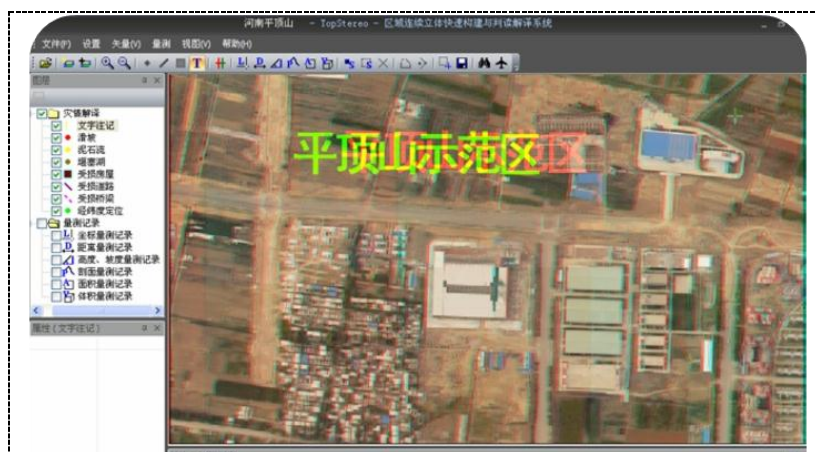
Figure 2. Regional continuous three-dimensional model in Pingdingshan area, which can be demonstrated with specific glasses.

Table 5. Obvious feature point coordinates differences in regional continuous three-dimensional model and GPS measured points.

	$\triangle X$	$\triangle Y$	$\triangle Z$
Max(m)	0.4	0.52	0.68
Mean(m)	-0.007	0.026	0.15
Standard Deviation (m)	0.18	0.25	0.36

Digital surface model depicts the elevation of the top surfaces of bare earth, buildings, trees, and other features above the bare earth. The experimental data were obtained by high precision light small aerial remote sensing system with operation mode 2 in Pingdingshan. Using LiDAR system and IMU/GNSS system, with the point density of 2.5 points per square meters, digital surface model precision meets the 1:2 000 topographic map accuracy specifications with processing speed of $0.5h/km^2$.
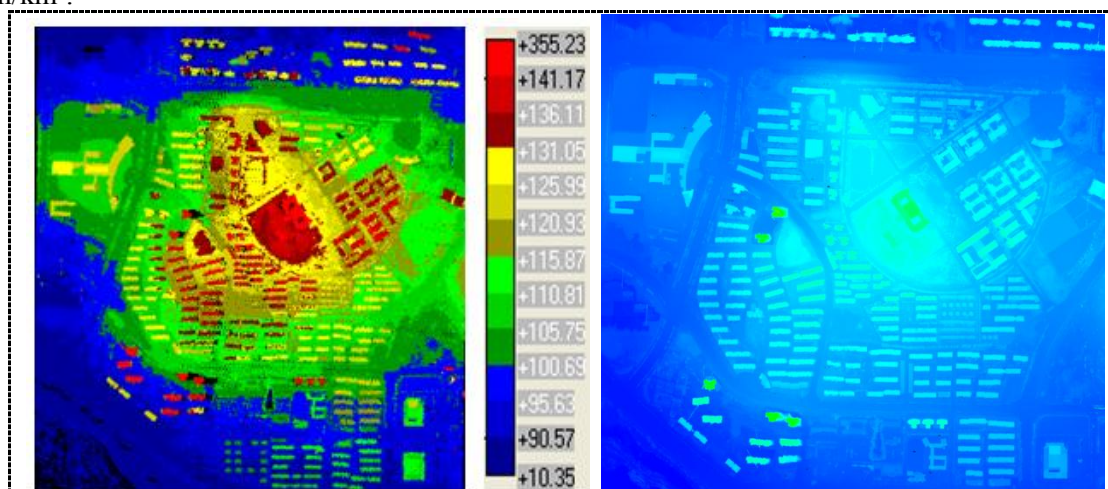

Figure 3. Point type digital surface model and grid type digital surface model in Pingdingshang area

5. Conclusion

This paper presents three experiments with three operation modes of the high precision light small aerial remote sensing system. The first mode is for large scale mapping, the second mode for digital surface model producing and the last mode for regional continuous three-dimensional modelling. The experiments fully demonstrate advantages of the aerial system, such as high precision and rapid response. It is also showed that without control points, the topographic maps meet 1:500 accuracy requirements. Two fast response mapping products- regional continuous three-dimensional model and digital surface model meet 1:2000 accuracy requirements.

   Further research will also carry out the applications of the high precision light small aerial remote sensing in different areas.

References

[1]   Ma H C and Sun J 2011 Intelligent optimization of seam-line finding for orthophoto mosaicking with LiDAR point clouds *Journal of Zhejiang University-Science C(Computers & Electronics)* **12** 417

[2]   Zeng Y W, Liang Y, Jiang W C and Wang X J 2011 *Computer and Computing Technologies in Agriculture* (Beijing: Scientific) p 176

[3]   Cui Y, Zhao X A 2010 *2010 International Conference on Remote Sensing* (Hangzhou: Scientific) p 275

[4]   Andreas N, Stanislav G and Dorit B 2011 *Geo-Spatial Information Science* **14** 85

[5]   Liu J N, Zhang X H 2003 Progress of Airborne Laser Scanning Altimetry *Journal of Wuhan Technical University of Surveying and Mapping(WTUSM)* **28** 132